Bachelor Thesis

Degree Project in Marine Geology 30 hp

Sedimentary structures and origin of deep-sea turbidites at The North Pole

Viggo Håkansson

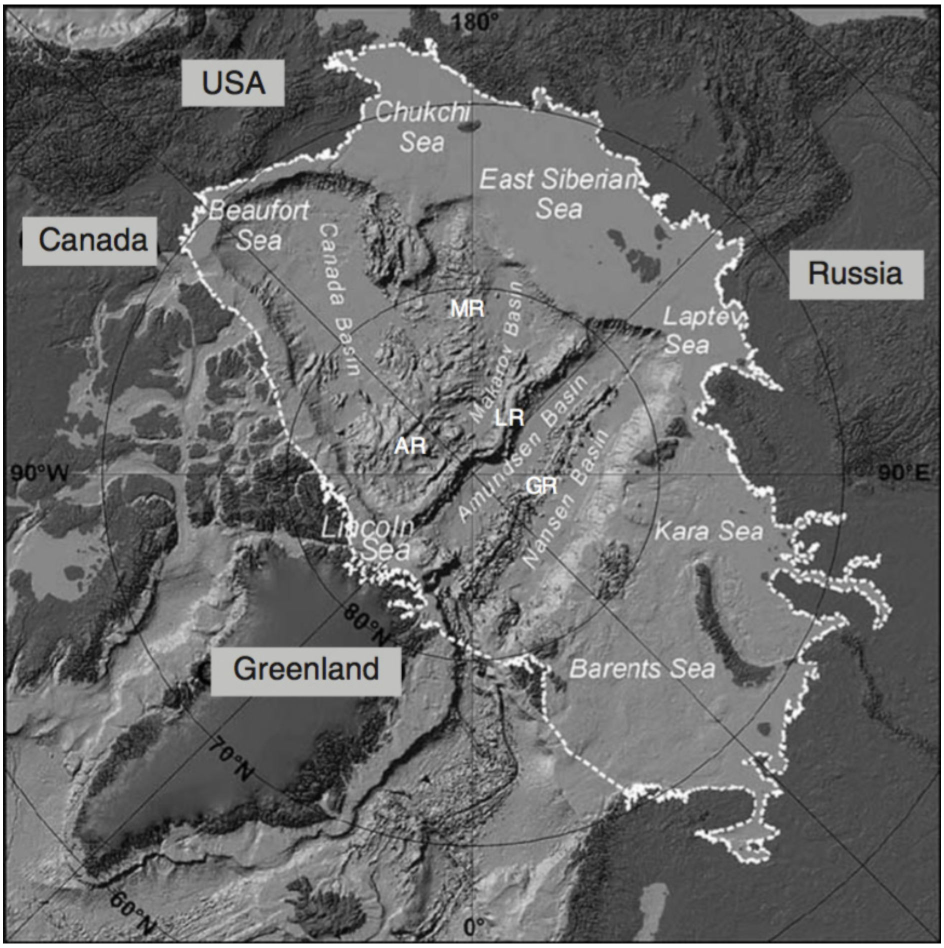

Stockholm 2016

Department of Geological Sciences
Stockholm University
SE-106 91 Stockholm
Sweden

Sedimentary structure and origin of deep sea turbidites at the North Pole

Abstract

This project examines the sedimentary characteristics of the LOMROG III core PC11 from 2012, taken near the geographical North Pole. Previous work has suggested that an extensive sequence of turbidites exists at the North Pole, and originate as glacial debris flows on the continental slope of Greenland. Grain size data, magnetic anisotropy (AMS) and X-ray fluorescence scanning (ITRAX-XRF) are combined to determine the sedimentary structure and origin of these turbidites. The objective is to find common geochemical signatures in the lithologies and to determine magnetic fabric orientation, to test whether individual turbidites show a common paleoflow direction and share a common mineralogical provenance.

Introduction

Mass Wasting, Turbidites and The Burma Sequence.

Boggs (2006) describes a turbidite as a sedimentary deposition from a turbidity current, which is a type of subaqueous sediment gravity flow (Figure 1). Turbidity currents commonly originate on continental margins and particularly in or in proximity to the heads of submarine canyons. They are a form of turbulent density current that flow downslope along the bottom of an ocean or a lake as a result of a density contrast with the surroundings. These flows often originate from the abyssal slope and are the result of breakdown in grain packaging and internal deformation of the sediment mass. The range, speed and volume of these flows are significant and they are capable of transporting large quantities of sediment far out into the deep ocean. Since the deep ocean receives little sedimentation from other sources, turbidity currents are a major source of sediment to these areas (Stein, 2008).

A turbidity current is usually initiated by a significant event such as an earthquake or storm waves acting on the continental shelf. Such an event may entrain sediment that starts to move down slope, eroding and picking up increasing amounts of sediment with increasing speed (Boggs, 2006).

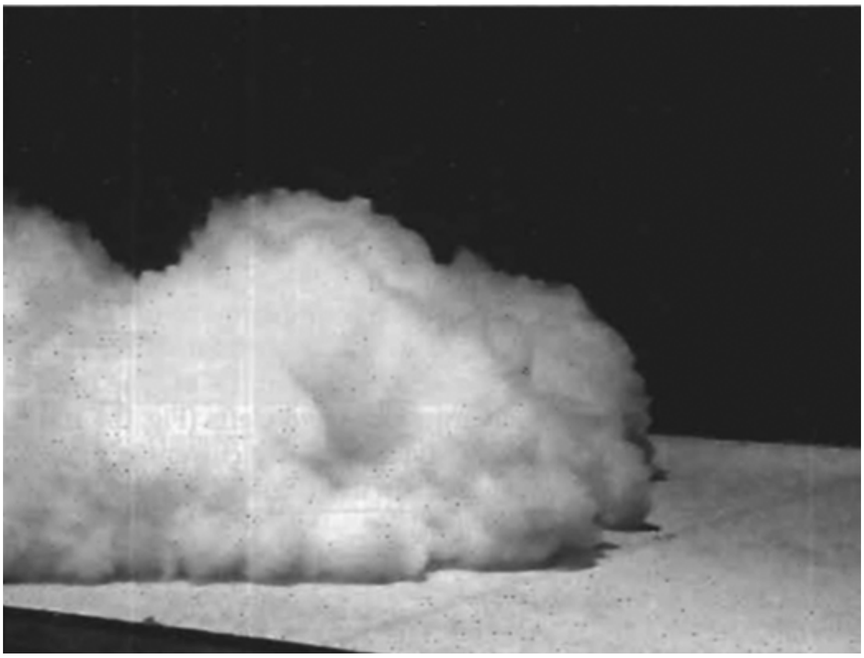

Figure 1: A lab generated turbidity current. Picture from Principles of sedimentology and stratigraphy (Boggs, 2006).

The flow will gradually lose speed until the sediment load has settled. As the speed of the flow slows, the water loses its ability to entrain particles. Since heavier particles require faster flow speed to remain suspended, they settle before lighter particles and a characteristic fining upwards sequences, known as a turbidite, is deposited (Boggs, 2006).

A. H. Bouma proposed that an ideal turbidite sequence commonly called a *Bouma sequence,* consists of five structural units that include characteristics of several subtypes of turbidites (Boggs 2006) (Fig. 2). These stuctural subdivisions are believed to contain the record of flow strength decay and the gradual development of the different sedimentary structures as the current loses strength (Boggs, 2006). Most turbidites do not contain all of the A to E sequences. Many turbidites lack the basal A unit or the upper D unit (Boggs, 2006). Furthermore, Unit E is difficult to differentiate from normal hemipelagic sedimentation.

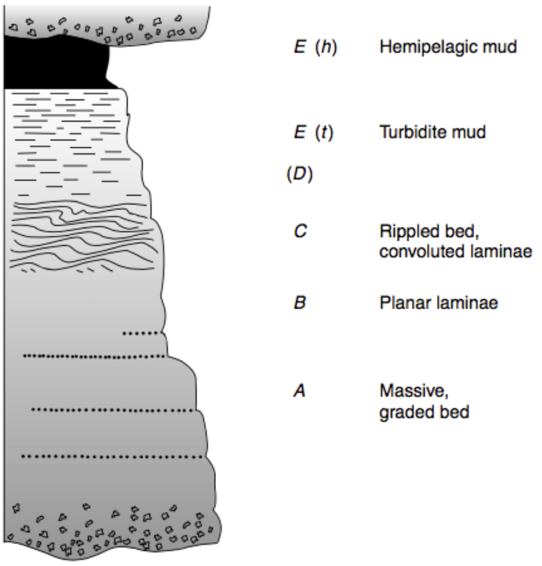

Figure 2: Graded bedding of a turbidite divided according to the Bouma sequence. Picture from Earth Structures (Van der Pluijm and Marshak, 2004).

Turbidite depositional environments

Turbidite flows from the continental margin spread outward from their source area onto the deep sea floor where they leave a broad cone-shaped fan known as an abyssal fan. Topographical features of the ocean floor such as ridges, canyons and rises will influence the direction and shape of the flow (Stein, 2008). The initial force of a turbidite is erosional and the turbidite flow leaves a channel in its wake. This means that the turbidite can create a system of channels that serves as a pathway to the area of deposition. Besides turbidites, other mass wasting processes such as slumps, creep and sliding appear to be a source of large-scale mass transport of sediments on steep continental slopes and ridges (Figure 3). While bearing similarities to turbidite flows in their origin, they retain some cohesion during the movement and don't reach as far out to sea (Boggs, 2006).

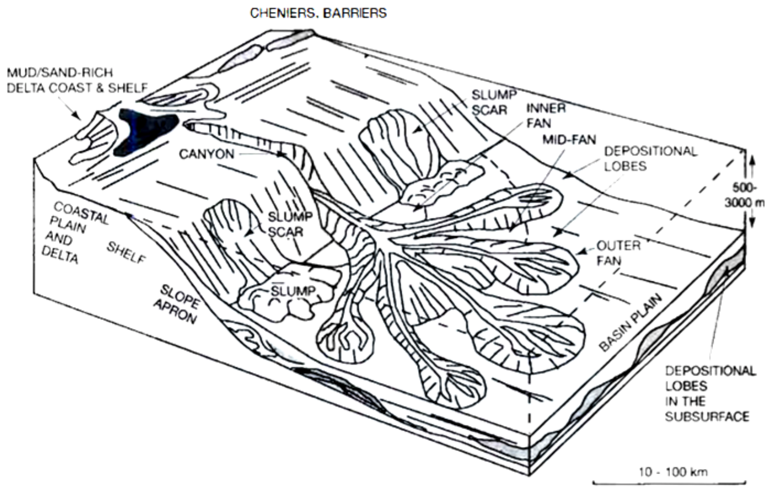

Figure 3: Depositional model for a point-source sand-rich submarine fan. Picture from Boggs 2006.

The Arctic Ocean

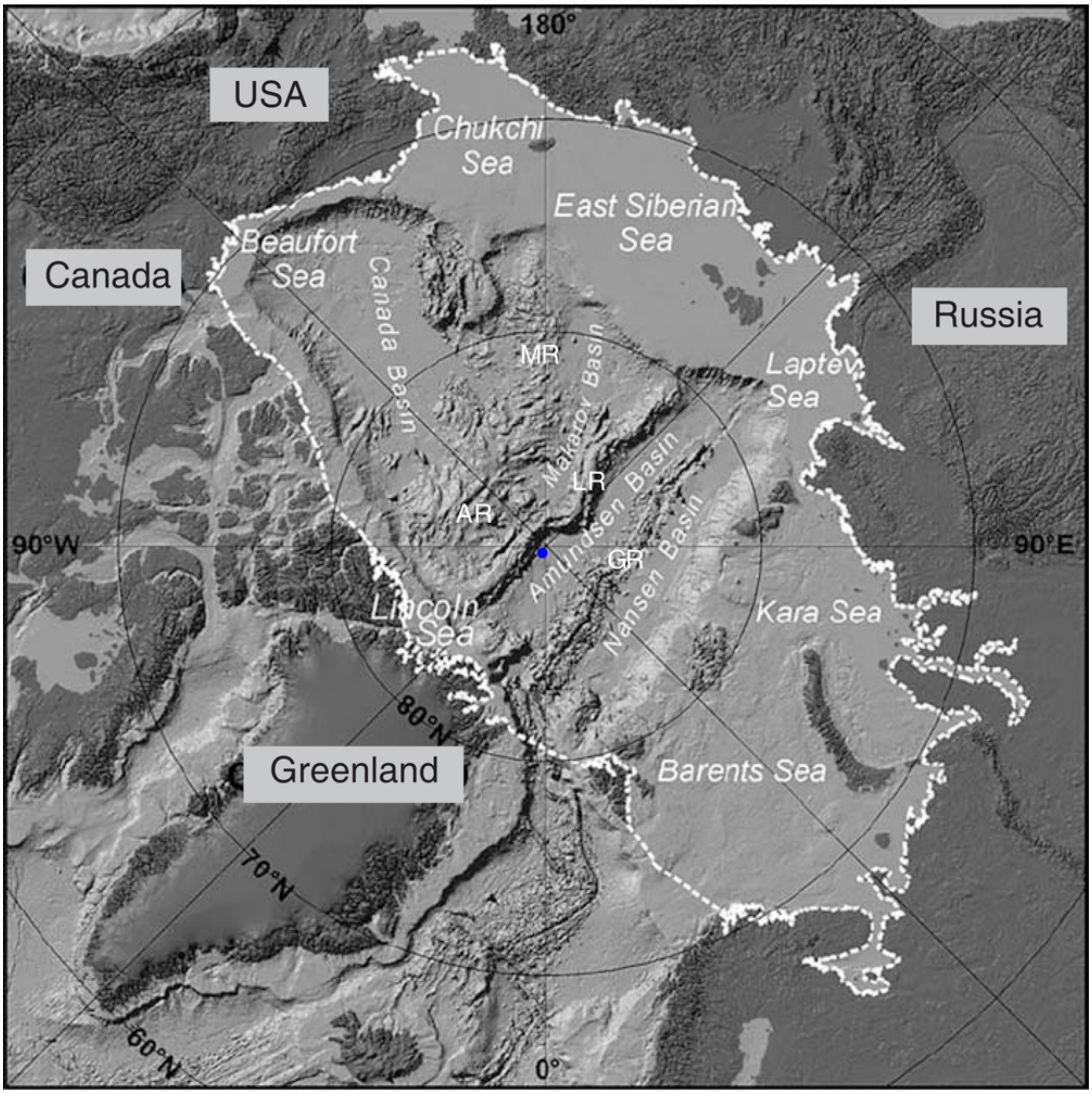

Figure 4: The Arctic Ocean, its shallow marginal seas, and major basins. GR, Gakkel Ridge; LR, Lomonosov Ridge; AR, Alpha Ridge; MR, Mendeleev Ridge. LOMROG III PC11 core sampling location marked in blue. Picture from Stein 2008.

The Arctic Ocean is one of earth's five major oceans. It is surrounded by vast marginal seas and has several deeper basins separated by complex geological structures of very different origin. One of these basins is the Amundsen Basin located between the Lomonosov Ridge and the Gakkel Ridge (Stein, 2008).

The Lomonosov Ridge

The Lomonosov ridge is a >1800 km long continental fragment that was rifted from the Eurasian continental margin by seafloor spreading in the early Cenozoic. The shallower parts of the ridge reach depths of 700 to 1000 meters below sea level (mbsl) and bear the scars of iceberg erosion (Kristoffersen, et al. 2007) and scouring marks that are interpreted as signs of grounded ice shelves (Jakobsson et al. 2016.).

Deep sea turbidites at the North Pole

On the bathymetric highs of the central Arctic, sea ice is considered the dominant transport agent for terrigenous sediments. However, in the deep basins and the abyssal plains, there is ample evidence for large-scale input of sediments from turbidity currents (Stein, 2008).

During the Pleistocene ice sheets have advanced and retreated over the northern hemisphere in a series of glacial and interglacial cycles. In the present time there are no areas of the Arctic where ice is grounded to the continental shelf. This is in stark contrast to full glacial periods when ice sheets moved across the shelves, and carved deep troughs across the shelves where ice streams were active. Advancing ice sheets thus greatly increased the rate of sedimentation to the continental slopes (Stein, 2008).

The process of sediment build-up by ice and eventual mass wasting is described by Stein (2008) in a three stage conceptual model. The first stage is during full glacial periods when massive sedimentation by ice streams reaches the shelf break, which causes upper slope instability and downslope mass wasting with accumulation in trough mouth fans. The second stage is between ice streams where the sedimentation delivery rate to the continental slope is much lower and mass wasting takes place in the form of sediment slides. The third stage is where ice sheets do not reach the continental shelf break even during full glacial periods. It follows that sediment input in this stage remains low throughout the complete glacial-interglacial cycle. Here, large submarine channel systems created by debris flows are typical instead (Stein, 2008).

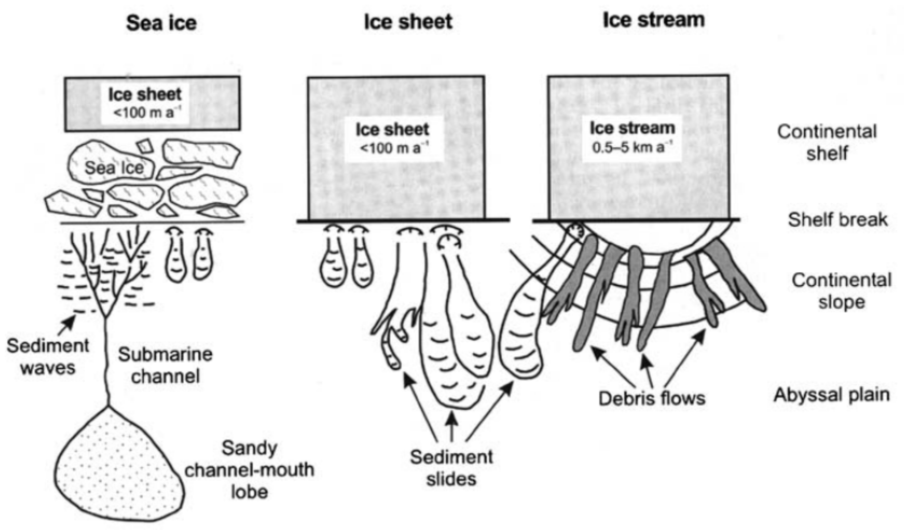

Figure 5: Conceptual model of ice dynamics and sedimentary products on a glacier-influenced continental margin. Picture from Stein (2008).

Other kinds of sedimentation include diamictons, which are characterised by unsorted to poorly sorted sediment with larger particles suspended in a finer grained matrix. The coarse fraction may include angular, faceted or striated pebbles. Hemipelagic sedimentation is also common in the deep sea. It consists of muddy sediment and forms close to continental margins, is slowly deposited and consists of terrigenous input from a combination of sources (Boggs, 2006).

The North Pole Submarine Fan

A submarine fan often consists of a series of stacked debris flows forming a prograding wedge close to the source of the sediment or some distance away in which case there often is a channel leading to the fan (Boggs 2006). In the Amundsen Basin such a channel system extends from the Lincoln Sea to the North Pole (Kristoffersen et al., 2004). These channels are likely pathways for turbidity currents originating from the Greenland coast. It follows that the sediment in the Amundsen Basin might very well have their provenance in the Lincoln Sea shelf (Stein, 2008). However, the provenance of the Amundsen Basin sediments is controversial. Kristoffersen et al. (2004) favour the theory that the turbidite sequences originate from the Lincoln Sea and base this assumption on bathymetric data. This data shows submarine channels originating from the Canadian-Greenland continental slope suggesting that this is a distal lobe of a submarine fan. They propose that this feature be named the "The North Pole Submarine Fan" (Figure 4). Kristoffersen et al. (2004) believe that the North Pole Submarine Fan developed mainly by increased sediment input to the margin of Canada and North Greenland during glacial periods, which then caused gravity driven sediment flows into the Amundsen Basin (Kristoffersen, Y. et al. 2004).

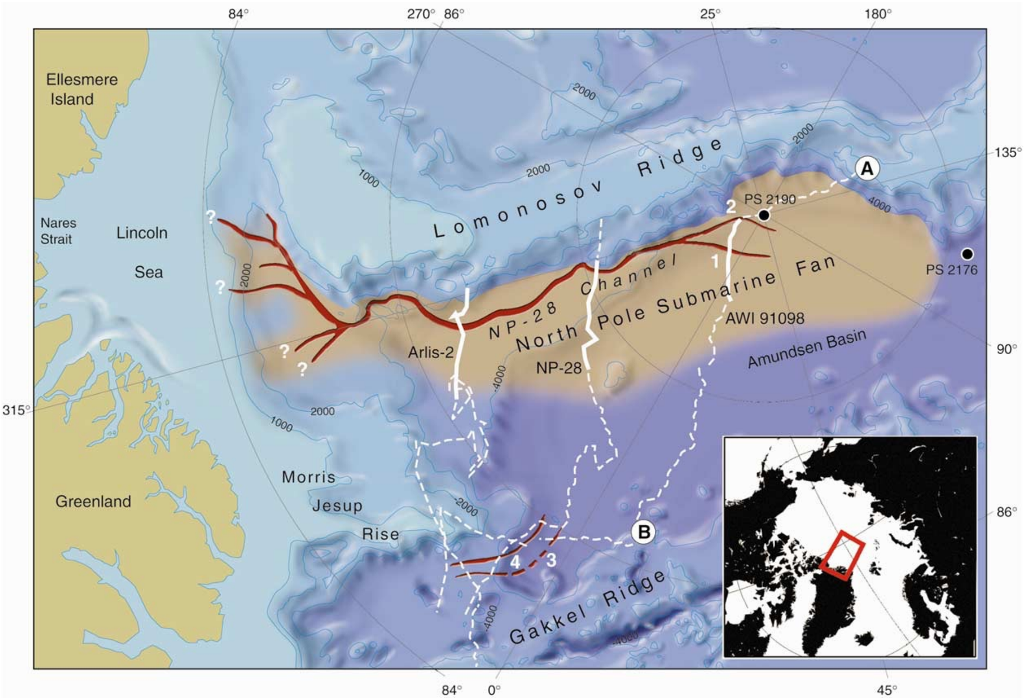

Figure 6: Map of the Amundsen Basin with the locations of seismic profiles and observed crossings of submarine channels. Major sediment pathways indicated by a bold dark red line and the outline of the North Pole Submarine Fan by dark brown colour. Picture from Kristoffersen (2004).

This hypothesis is however questioned by Stein (2008) who suggests the Eastern Laptev Sea as a possible source area for, at least, parts of the sedimentation. This is based on clay mineralogy from a core taken at the North Pole that first described the many stacked turbidite deposits in this region (Svindland, and Vorren, (2002).

Methods

The sediment core analysed as part of this study (LOMROG III PC-11) was taken on 2012-08-23 at 89°58'06 N 58°27'37.68 W at 4228 mbsl using a piston core. The core was divided into 5 sections. While the core was not geographically oriented, the individual sections are cut along their long axis in the same way, making them oriented with regards to each other.

X-ray fluorescence scanning

To determine the relative elemental composition of the sediments, X-ray fluorescence scanning (XRF-scanning) was performed using an ITRAX XRF machine. This method involves sending X-rays towards the sediment core and interpreting the fluorescent X-rays that is released from the material after initial bombardment. From this data, elemental ratios are calculated. Sections of the core were scanned after the top 1 mm layer of sediment had been scraped of in a perpendicular direction to the core length. Care was taken to minimize core surfaces exposure to air.

A Chromium X-ray tube was used for superior signal to noise ratio, and the machine was set to 30 kV, 55 mA for 100 s. The data was then summed to 100% and normalized for all the elements, to eliminate variability caused by differences in porosity and cracks. Then the data was normalized to aluminium. This method of normalization to aluminium was chosen since it would minimise influences arising from down-core changes in organic material content (Löwemark 2010) since proximal core PS2190-1 was noted to have high organic carbon in the sediments (Stein, 2008). Measurements were taken every 5 mm and data was collected for the elements Si, S, Cl, K, Ca, Ti, Mn, Al and Fe.

Magnetic Anisotropy

Anisotropy of Magnetic Susceptibility (AMS) is a geophysical method that uses magnetism as a proxy of the sediments fabric orientation. This data can be used to recreate paleoflow direction (Wassmer and Gomez, 2011). The AMS method is very sensitive and even very small variations in AMS can provide valuable and reliable information on sediment fabric orientations (Saganotti 2011).

During AMS measurements, a sediment sample is exposed to a magnetic field in three axes (Tauxe, 2002). The degree to which the sample can be magnetized is measured, resulting in a magnetic ellipsoid generated during this measurement. Magnetic anisotropy means that magnetic grains can be magnetized to a varying amount depending on the crystals orientation in the grain. Since magnetic moments prefer to be aligned head to tail, the magnetic anisotropy will be affected by grain orientation. The strongest direction will be the K_{max} and is the grains longest dimension. K_{min} is the grains shortest direction or “hard to magnetise” (Figure 5). K_{max} is also known as K1, and K_{min} is also known as K3

When sediments settle on the sea floor they are subject to imbrication and alignment to the current direction. It is therefore possible to evaluate grain orientation with AMS and draw conclusions about paleo-current.

Quiet water yields a K_{min} that is perpendicular to bedding and a K_{max} that is spread in the bedding plane (Figure 5). Moderate flow causes platy particles to imbricate and results in a clustering of K_{min} towards the flow direction and streaked K_{max} perpendicular to flow direction (Figure 5). A high velocity flow causes a streaked K_{min} and a clustered K_{max}. The reason for this is that the elongated grains roll with their long axis perpendicular to flow (Tauxe, 2002).

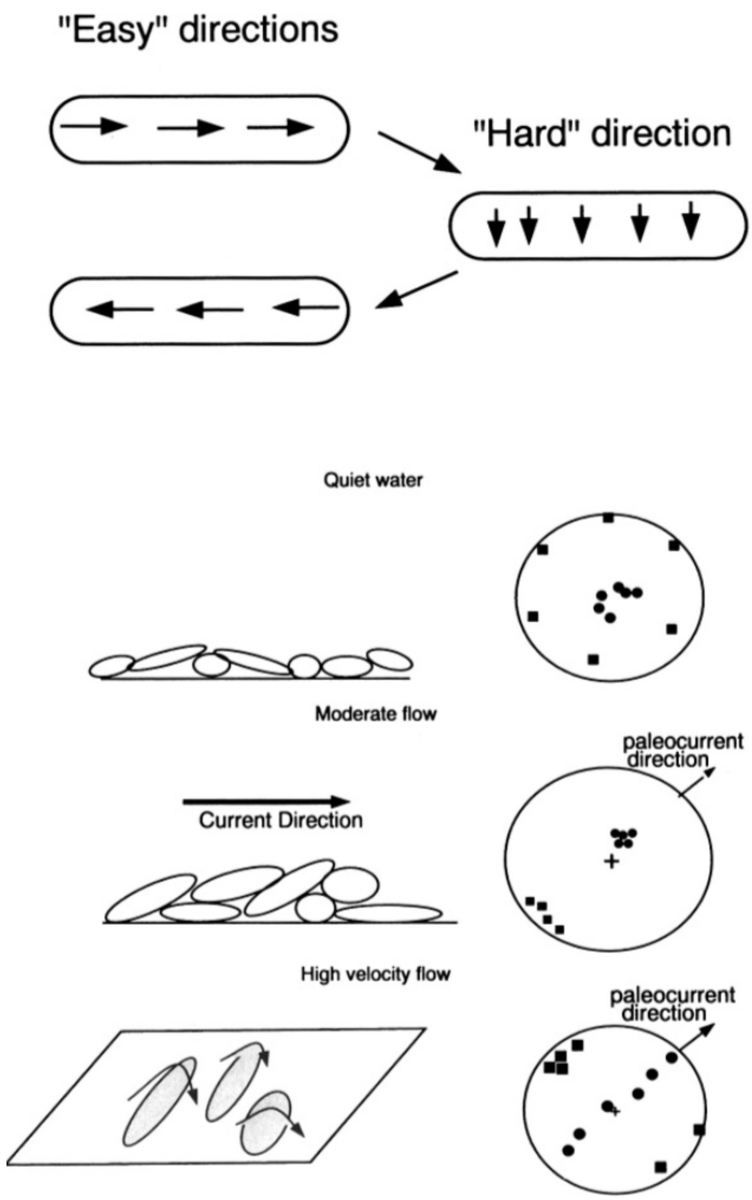

Figure 7: Upper – Magnetic anisotropy resulting from grain shape. Lower – How grains align with current direction and characteristics of AMS data projected on a sphere. Picture from Paleomagnetic principles and practice (Tauxe, 2002). Note that the stereonets are southern hemisphere projections.

Sampling for AMS measurements was done using 2x2x2 cm sampling cubes. They were inserted into the central part of the core and care was taken to minimize effects of core disturbance during sample removal. Areas of hard mud adjacent to areas of soft mud in the stratigraphy and concretions in the core did prove to make sampling difficult, but most samples had a large majority of sediment taken into the sampling cube without disturbance of the sediment. A total of 269 samples were taken. Cubes were individually marked with core, section and distance from core top. They were wrapped in wax tape when not used for testing, to minimize loss of liquid by evaporation.

AMS measurements were performed using a Kappabridge MFK1. The software was set to 976Hz and 425 amp/m. Calibrations were done before sampling and after each cleaning. Data was processed and mean tensor directions were calculated using the Ansisoft 4.2 software package.

Grain size

The grain size data was previously acquired at the Department of Geological Sciences at Stockholm University. These measurements were done with the Malvern Mastersizer 3000, which uses laser diffraction to analyse particle size distribution. Average distributions are reported from 5 measurements taken at 2 cm intervals throughout the core.

Results

Grain size

The result of the grain size data (Figure 8) displays the grain size distribution for the sediment. Grain size data that clearly display different lithologies was chosen and an X-ray picture of the core sections is included. In the 2-10 µm and 10-63 µm, 20 areas of turbidites are evident and labelled T1-T20. These display a coarse base and a fining upward pattern with a sharp contrast. Grain size is characterised by a reduction in 10-63 µm, and an increase in 2-10 µm fractions up-core. For diamicton there is a large increase in the >63 µm fraction, compared to the other lithologies. Diamicton (D1-D2) also has a fairly homogenous mix of grain sizes, which is evident in the kurtosis values. The hemipelagic sediment sequences (H1-H2) have a majority of 2-10 µm grains and a very varied kurtosis curve.

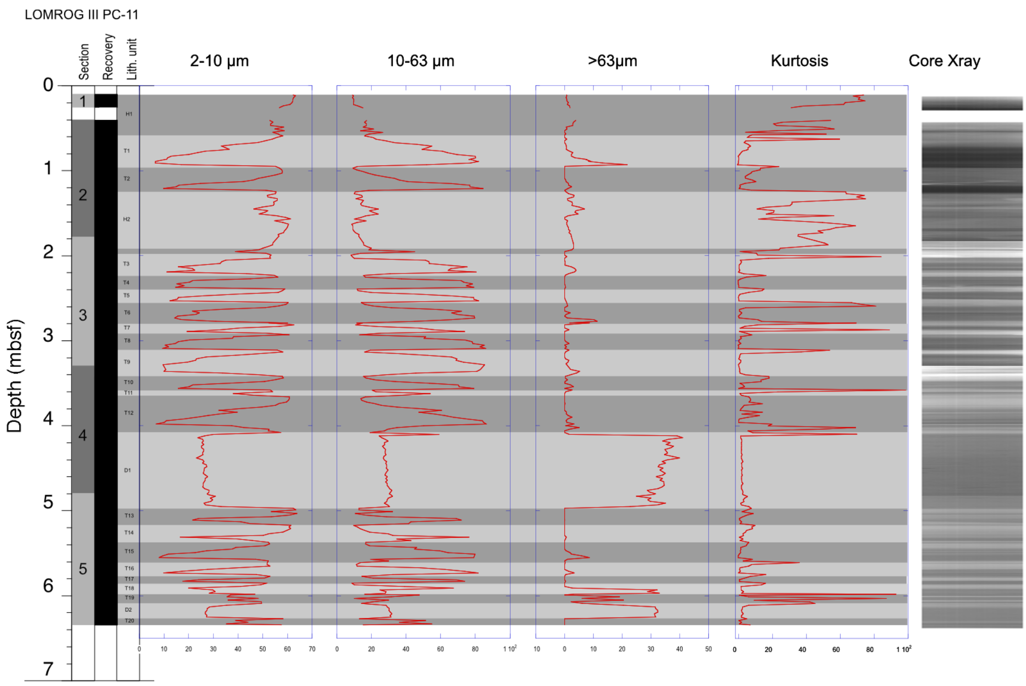

Figure 8: Grain size and core x-ray. Units are percentage.

ITRAX-Scanning data

After processing, the elemental ratios of Ca, Si and K were found to track the major lithological changes that were first identified by the grain size data, and are displayed here (Figure 9). These elements are also less sensitive to redox driven post-depositional changes and migration in the sediment layers (Libes, 2009).

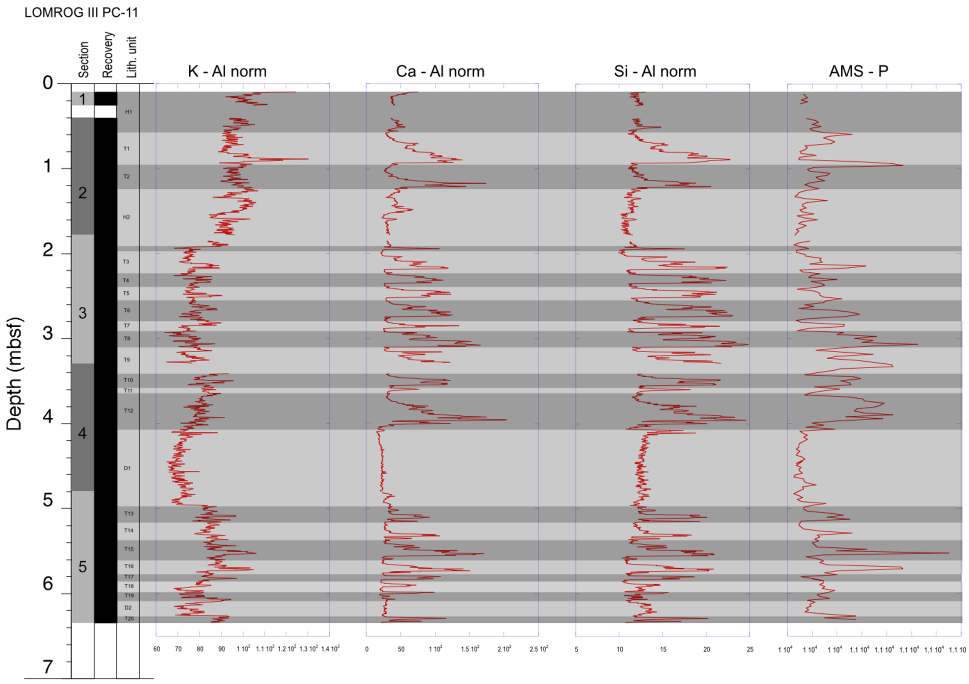

Figure 9: XRF and AMF P value (K1/K3). Units in CPS for XRF data.

From the XRF data a pattern very similar to what is seen in the grain size data appears (Figure 9). The turbidite lithologies have an up-core decrease in Si and Ca while K remains stable. This geochemical signature is the same for all the turbidites. Furthermore the two diamicton sequences show a similar chemical signature, as do the two hemipelagic sequences.

Anisotropy of Magnetic Susceptibility

The P value (ratio of K1/K3) from AMS measurements (Appendix B) also captures the patterns found in the grain size and XRF data is evident (Figure 9). Several derived AMS parameters were evaluated but the P value was chosen because it clearly demonstrates the turbidite pattern seen in the grain size chart. This data captures a flow speed pattern in the turbidite sequences that would signify a higher flow speed at the bottom of the turbidites that gradually decrease up-core. Diamicton and hemipelagic sequences display very little flow speed pattern.

A wind rose diagram of the AMS data (Figure 10) displays the estimated paleoflow direction for the turbidites. T11, T19, and T20 were omitted because there was not enough data to calculate mean flow direction. The T7 paleoflow direction was inconclusive and was also omitted in the wind rose diagram. Paleoflow estimation was done with the assumption of moderate flow waters as described by (Tauxe, 2002).

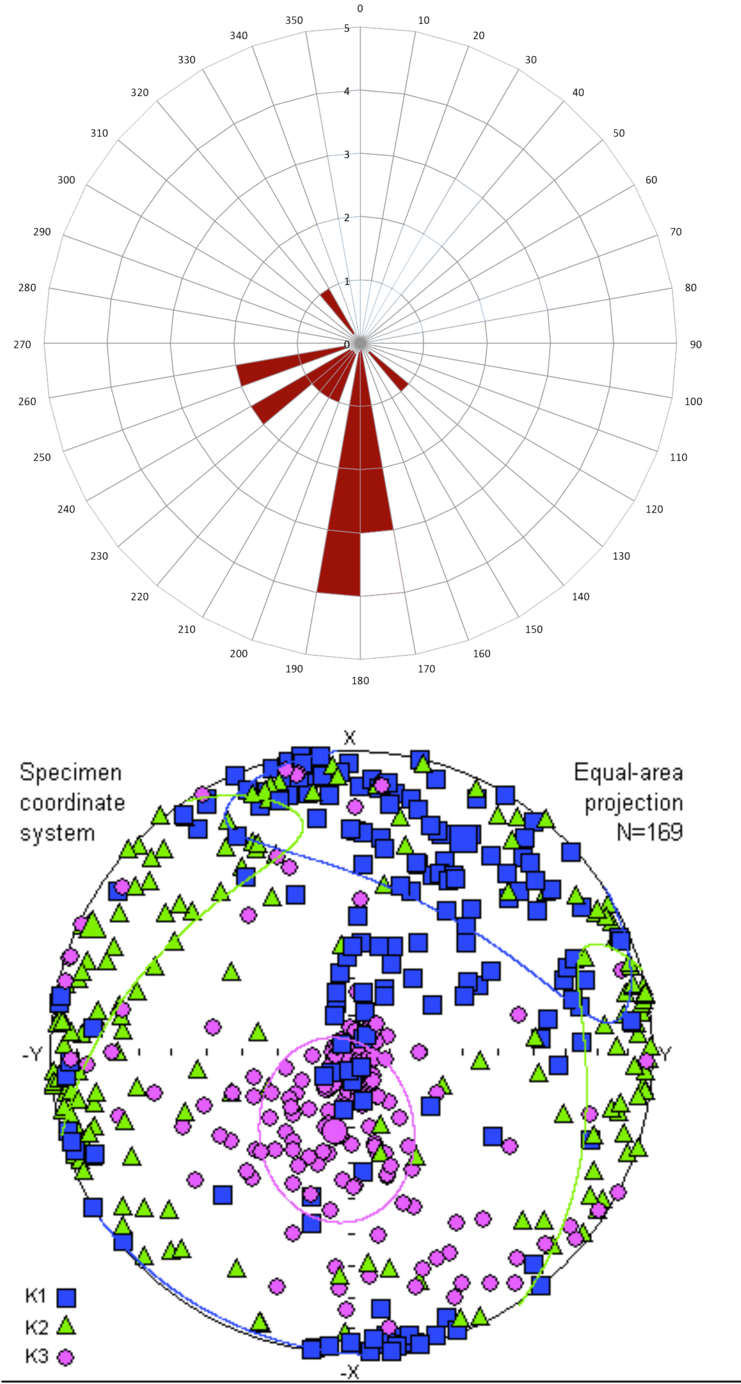

Figure 10: Upper: Wind Rose diagram displaying the direction of the estimated turbidite paleoflow direction and amount of turbidites with that direction. Values are rounded to 10 degrees. Note that the degrees don't correspond to a geographical direction. Lower: a stereonet displaying all AMS values from all T1-T20, with confidence ellipse (circles) and mean direction (larger symbol).

Discussion

The goal of this study was to examine the sedimentary characteristics (magnetic fabric) and geochemical signatures (ITRAX XRF-scanning) in turbidites recovered from the North Pole, to assess whether they had a common source region.

Lithological classification

When examining the data, three different lithological patterns emerge and the classifications are displayed in appendix A. These are turbidite, diamicton and hemipelagic sediment.

Turbidite

The grain size distribution clearly shows several fining upward, sharp contrast, patterns consistent with several turbidity current deposits. Additionally, the XRF data shows a similar down-core increase pattern in the distribution of elements in a turbidite sequence. Ca peaks at about 7 times the Si value indicating calcium rich sediment. There is also the classical fining-upwards visual signature on the core surface. These are all signs of a turbidity flow deposition known as a turbidite. Additionally the AMS P value displays a pattern of up-core reduced flow speed, which would be expected in the gradually declining flow of a turbidity current.

Figure 11: Top of section 3 showing a fining upward cycle on the core surface. Turbidite T10.

Diamicton

A second lithological classification is diamicton, seen in D1 (depth interval 4,08-4,98 m). This conclusion is supported by the grain size data showing an unsorted grain size distribution throughout the sequence with a higher content of larger particles. Angular pebble to granule size fragments are visible in the diamicton intervals in the X-ray of the core. Furthermore the AMS data indicates a very scattered grain orientation, which is in stark contrast to the turbidite grain orientation, and expected for a diamicton.

The D2 sequence (depth interval 6,06 – 6,28 m) is similar to D1 but does not display the ample angular fragments in the X-radiograph, but rather granule size particles. The AMS stereogram data for D2 indicates some grain orientation indicative of a slight current (Appendix B). While the classification for this lithology remains diamicton, the case for D2 is less sustained than for D1.

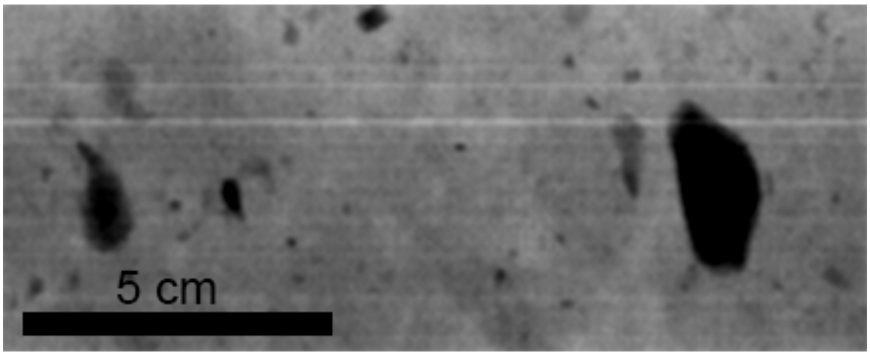

Figure 12: X-ray showing larger angular fragments in D1 from.

Hemipelagic sediment

The hemipelagic sedimentation classification is supported by the grain size data showing that fine silt to mud size particles dominates. The kurtosis of the hemipelagic parts is also very much different from the diamicton. As with the diamicton, the AMS data shows a random grain orientation, further differentiating these units from the turbidites. The cross-plot in appendix D indicates a similar chemical signature for both the hemipelagic sequences that differentiate them from other lithological units (Appendix D). It is difficult to set a clear boundary between hemipelagic sedimentation and the top layer of a turbidite, which is why this classification is not without some uncertainty.

The different turbidite sequences were clearly identified in the grain size, elemental and AMS data. For the AMS data, the P value, which is the ratio of K1/K3, most clearly captured the turbidite sequences. This is because the grains are oriented in the declining current speeds of the turbidity current. In quiet water the grains will imbricate and point K1 in random directions, causing the K1 tensors to cancel each other out. This yields a lower P value. Whilst in a moderate flow the K1 will cluster, thus increasing their resulting value in the K1/K3 equation. This pattern is even more evident in a deposit from a stronger flow, where the K3 vector will be less concentrated while the K1 vector is still clustered, giving the highest P value. Thus a flow speed pattern is visible in the AMS data. However, this only provides a relative orientation, suggesting that most of the turbidites can from generally the same direction. However, since the core was not oriented it is not possible to draw direct conclusions as to the geographical direction of these flows.

In some instances, core disturbances may have impacted the quality of the AMS data. In figure 9, core disturbance is visible and most likely caused by friction against the core liner. While the sample was taken from the middle of the core, it is reasonable to assume that the disturbance is conical in shape. Hence there might be some systematic disturbance of the sediment since the underlying sediment could have an angle corresponding to the core disturbance. Splitting the cores might cause expansion in the core liner and disturbance of the sediment, however this effect should be minimal since the samples were taken from the centre of the core (Shimono et al. 2014).

Possible provenance

The AMS fabric data strongly supports the notion that the turbidites originated from a similar direction, and not a mixture of deposits formed from the Siberian and Greenland margins. While the paleoflow direction does have a major direction, some turbidites suggest another one. Two turbidites stand out from the rest; T10 indicates paleoflow in an almost 90 degree angle from the mean direction. The stereogram projection for T10 does display a pattern that could be the result of a high speed current. In this case the paleoflow direction would be in parallel to the K3 indicators. The T10 turbidite still have a similar chemical signature as the other turbidites. Since the chemical signature is similar for the T1-T20, it supports the idea that they are from the same provenance. One could hypothesise that originate from dolomites in North Greenland (Stein 2008).

T1 has a remarkable pattern as well. It seems to indicate that the grains are standing upright, which is unseen in the other turbidites, and may be a result of sampling disturbance, in the soft, near-surface sediments.

As for the diamicton, a most likely provenance is the Lomonosov Ridge. This is echoed by Svindland and Vorren (2002) who examined a similar diamicton sequence in the proximal Core PS2190-1, and hypothesized that the diamicton is a result of downslope transport from the Lomonosov Ridge as a submarine debris flow. An idea that is contested by Stein (2008) who argues that the diamicton is the result of major and rapid glacio-marine sedimentation event from sea ice or icebergs. The provenance of the hemipelagic sediment is difficult to hypothesise over since it can be ice rafted from any part of the Arctic Ocean, aeolian or gravity transported from the nearby continent. It is likely that all these factors play some part.

Conclusion

The stratigraphy in the LOMROG III PC11 core can be classified into 3 major lithological types. Turbidites of which there are 20, diamicton numbering 2 and hemipelagic sedimentation also numbering 2. These all have differences in their Ca to K ratio, grain size distribution, and magnetic fabric orientation. The AMS data suggests that most of the turbidites exhibit a similar flow direction. They seem to have a similar geochemical composition, with elevated amounts of calcium that may indicate large inputs of dolomite. Dolomite is commonly associated with Northern Canada and Greenland, and suggests that this could be a source region for the turbidites. A more detailed mineralogical analysis is needed to confirm this, and a wider comparison with XRF-scanning data from other cores on the LR to establish this.

References

Boggs, S. (2006). *Principles of sedimentology and stratigraphy*. New Jersey: Prentic Hall.

Libes, S. (2009). *Introduction to marine biogeochemistry*. New York: Elsevier Inc.

Stein, R. (2008). *Arctic ocean sediments*. Amsterdam: Elsevier Science.

Van der Pluijm, B. and Marshak, S. (2004). *Earth structure*. New York: W.W. Norton.

Löwemark, L. Chen, H. Yang, T. Kylander, M. Yu, E. Hsu, Y. Lee, T. Song, S. Jarvis, S. (2011) *Normalizing XRF-scanner data: A cautionary note on the interpretation of high-resolution records from organic-rich lakes.* Journal of Asian Earth Sciences, 40 p. 1250-1256

Kristoffersen, Y. Coakley, J. Hall, K. Edwards, M. (2007) *Mass wasting on the submarine Lomonosov Ridge, central Arctic Ocean*. Marine Geology 243(1-4), p.132-142.

Kristoffersen, Y. Sorokin, M. Wilfried, J. Svendsen, O. (2004) *A submarine fan in the Amundsen Basin*, Arctic Ocean. Marine Geology 204 p. 317-324.

Tauxe, L. (2002). *Paleomagnetic principles and practice*. Dordrecht: Kluwer Academic Publishers.

Sagnotti, L. (2011) *Magnetic Anisotropy*. Encyclopedia of Solid Earth Geophysics.

Shimono, T. Yamazaki, T. and Inoue, S. (2014). *Influence of sampling on magnetic susceptibility anisotropy of soft sediments: comparison between gravity and piston cores*. Earth, Planets and Space, 66(1), p.3.

Svindland, K. Vorren, T. (2002) *Late Cenozoic sedimentary enviroments in the Amundsen Basin*, Arctic Ocean. Marine Geology 186, p.541-555.

Wassmer, P. Gomez, C. (2011) *Development of the AMS method for unconsolidated sediments. Application to tsunami deposits*. Géomorphologie 3, p.279-290.

Marcussen, C. (2016). *LOMROG III Cruise report*. [online] Available at: http://a76.dk/xpdf/lomrog-III_cruise-report.pdf [Accessed 13 Mars 2015].

Appendix

Appendix A – Table of lithological classifications and units

Turbidite	Top (cm)	Base (cm)	Lithology
T1	58	96	Very dark brown silty clay
T2	96	126	Very dark olive brown silty clay
T3	198	224	Dark olive greyish sily clay
T4	224	240	Dark greyish mottled clay
T5	240	258	Olive brown slightly mottled clay
T6	258	280	Dark greyish clay
T7	280	292	Very dark grey clay
T8	292	310	Dark grey clay
T9	310	342	Dark grey some core disturbance
T10	342	358	Very dark grey silty clay
T11	358	364	Dark grey clay
T12	364	408	Dark grey clay
T13	498	517	Dark grey clay
T14	517	537	Very dark clay
T15	537	560	Very dark clayey silt
T16	560	577	Olive dark clayey silt
T17	577	586	Dark olive grey silty clay
T18	586	598	Dark grey sandy clayey silt
T19	598	608	Olive brown silty clay
T20	627	634	Dark grey silty clay

Diamicton	Top (cm)	Base (cm)	Lithology
D1	408	498	Very dark clayey sandy silt
D2	608	628	Olive grey silty clay

Hemipelagic	Top (cm)	Base (cm)	Lithology
H1	10	58	Dark brown greyish silty clay
H2	126	192	Dark brown silty clay

Lithological units. Depth values in centimetres below sea floor

Appendix B – AMS stereograms

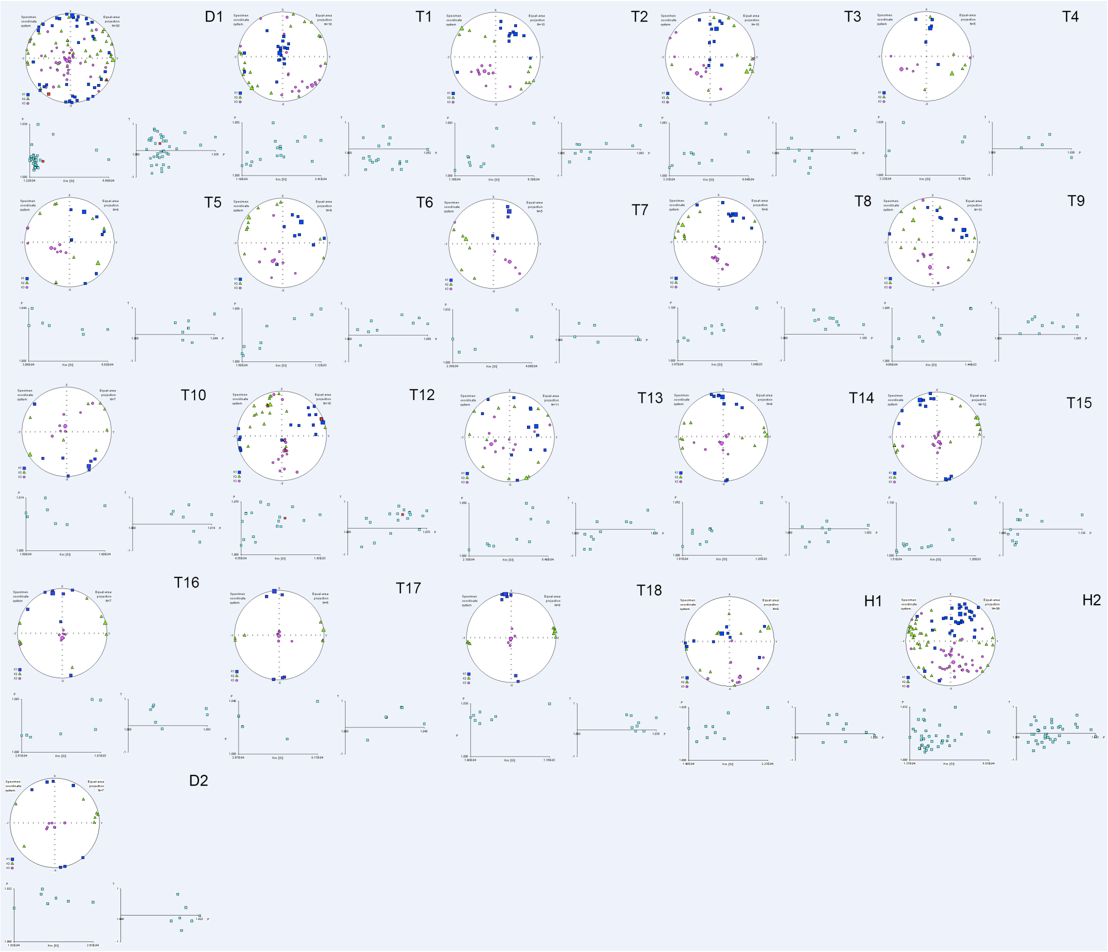

AMS stereogram. Large symbol is mean direction.

Appendix C – AMS Equations

Table 1: *Equations defining the quantitative anisotropy factors. Numbers of default factors are in bold.*

Factor No.	Mathematical expression	Usual symbol
1.	$\frac{15}{2}\frac{(k_1-k)^2+(k_2-k)^2+(k_3-k)^2}{(3k)^2}$	
2.	$\exp\sqrt{2((n_1-n)^2+(n_2-n)^2+(n_3-n)^2)}$	P'
3.	$\sqrt{2[(n_1-n)^2+(n_2-n)^2+(n_3-n)^2]}$	lnP'
4.	$\frac{k_1}{k_3}$	P
5.	$\ln\frac{k_1}{k_3}$	lnP
6.	$100\frac{k_1-k_3}{k_1}$	
7.	$\frac{k_1-k_3}{k_2}$	
8.	$\frac{k_1-k_3}{k}$	
9.	$\frac{k_1}{k_2}$	L
10.	$\ln\frac{k_1}{k_2}$	lnL
11.	$\frac{k_1-k_2}{k}$	
12.	$\frac{2k_1}{k_2+k_3}$	
13.	$\frac{k_2}{k_3}$	F
14.	$\ln\frac{k_2}{k_3}$	lnF
15.	$\frac{k_1+k_2}{2k_3}$	
16.	$\frac{k_1+k_3}{2k_2}$	
17.	$\frac{2k_2}{k_1+k_3}$	
18.	$\frac{1-k_3}{k_2}$	
19.	$\frac{2k_1-k_2-k_3}{k_1-k_3}$	
20.	$\frac{(k_1+k_2)/2-k_3}{k}$	
21.	$\frac{k_2-k_3}{k}$	
22.	$\frac{k_1}{\sqrt{k_2k_3}}$	
23.	$\frac{k_1k_3}{k_2^2}$	
24.	$\frac{k_1-k_2}{(k_1+k_2)/2-k_3}$	Q
25.	$\frac{k_1-k_2}{k_2-k_3}$	
26.	$\frac{k_2-k_3}{k_1-k_2}$	
27.	$\arcsin\sqrt{45\frac{k_2-k_3}{k_1-k_3}}$	
28.	$\frac{k_2^2}{k_1k_3}$	E
29.	$k_2\frac{k_1-k_2}{k_1(k_2-k_3)}$	
30.	$\frac{k_2/k_3-1}{k_1/k_2-1}$	
31.	$\frac{2n_2-n_1-n_3}{n_1-n_3}$	T
32.	$\frac{2k_2-k_1-k_3}{k_1-k_3}$	U
33.	$\frac{k_1+k_2-2k_3}{k_1-k_2}$	
34.	$\frac{\sqrt{((k_1-k)^2+(k_2-k)^2+(k_3-k)^2)/3}}{k}$	R
35.	$(k_1k_2k_3)^{\frac{1}{3}}$	
36.	$\frac{k_3(k_1-k_2)}{k_1(k_2-k_3)}$	
37.	$\frac{k_3(k_1-k_2)}{k_2^2-k_1k_3}$	
38.	$\frac{(k_1-k_2)(2k_1-k_2-k_3)}{(k_2-k_3)(k_1+k_2-2k_3)}$	

Appendix D – Chemical signature Cross Plot

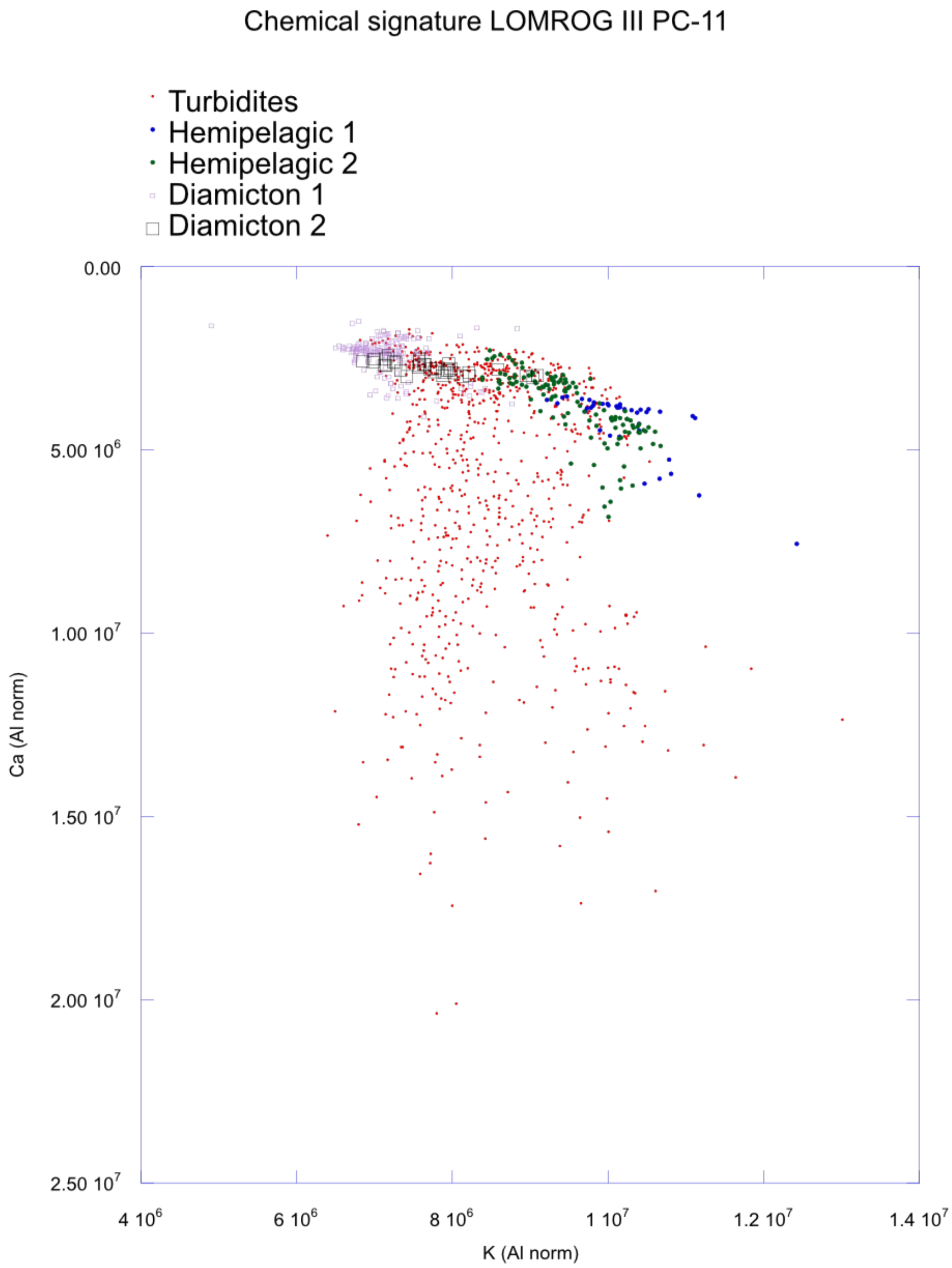

Appendix E – Chemical signature

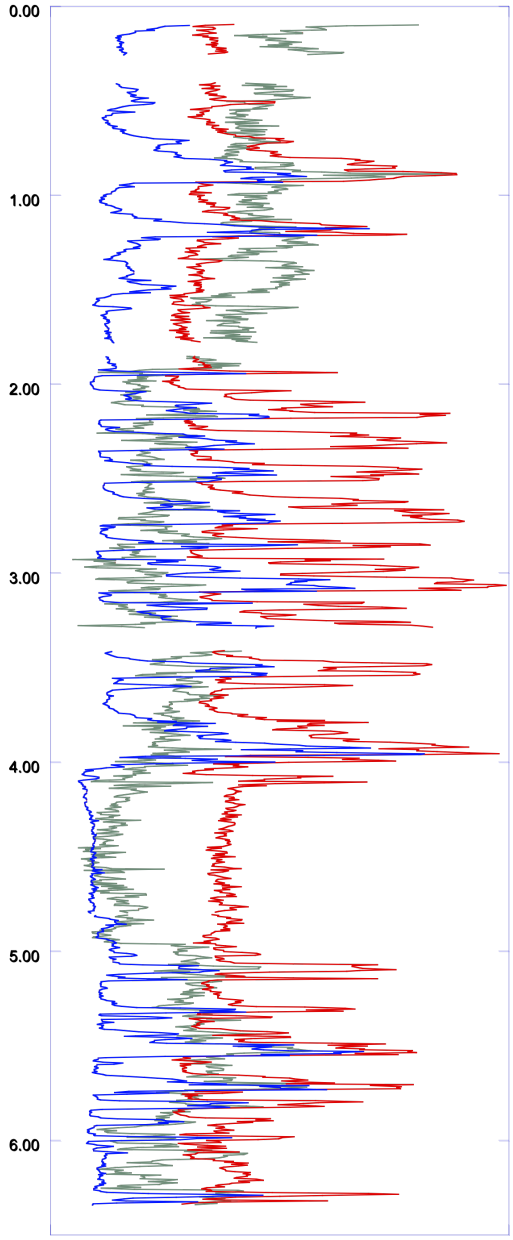

Chemical signatures. Green = K, Blue = Ca, Red = Si. Note that charts lack X value.